



CO and CO₂ methanation over M (M=Mn, Ce, Zr, Mg, K, Zn, or V)-promoted Ni/Al@Al₂O₃ catalysts

Thien An Le, Jieun Kim, Jong Kyu Kang, Eun Duck Park*

Department of Chemical Engineering and Department of Energy Systems Research, Ajou University, Suwon 16499, Republic of Korea

ARTICLE INFO

Keywords:

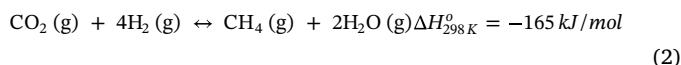
Ni
 γ -Al₂O₃
 Al@Al₂O₃
 CO methanation
 CO₂ methanation
 Promoter
 Mn
 Ce

ABSTRACT

Effects of metal promoter on CO and CO₂ methanation were examined over Ni-M (M = Mn, Ce, Zr, Mg, K, Zn, or V)/Al@Al₂O₃ catalysts prepared by the co-impregnation method. Ni-M (M = Mn, Ce, or Zr)/ γ -Al₂O₃ catalysts were also investigated for comparison. The prepared catalysts were characterized with a variety of techniques such as N₂ physisorption, CO₂ chemisorption, H₂ chemisorption, temperature-programmed reduction with H₂ (H₂-TPR), temperature-programmed desorption of CO₂ (CO₂-TPD), X-ray diffraction (XRD), high-resolution transmission electron microscopy (HRTEM), X-ray photoelectron spectroscopy (XPS), and in-situ diffuse reflectance infrared Fourier transform spectroscopy (DRIFTS). Among different promoters, Mn, Ce, Mg, V, and Zr are beneficial to enhance both CO and CO₂ methanation activity due to the improvement of the Ni dispersion. The Ni-V/Al@Al₂O₃ catalyst performs the highest CO methanation activity due to the largest Ni sites. However, it is not the best one for CO₂ methanation among tested catalysts because of the much decrease in CO₂ adsorption capacity. The promotional effect of Mn is the most remarkable for both CO and CO₂ methanation. On the other hand, the negative effect of K and Zn was observed on both CO and CO₂ methanation by the small number of active Ni sites and the decrease in the amount of basic sites. The CO₂ methanation mechanism over Ni-Mn/Al@Al₂O₃ catalyst is elucidated by the transform route: adsorbed carbonate species – formate species – methane under hydrogenation process.

1. Introduction

CO₂ utilization technology is an ideal solution to cope with CO₂ emission problem causing global warming effect [1]. Since CO₂ is the thermodynamically stable carbon-containing molecule, its chemical transformation requires other highly reactive chemicals such as epoxides and hydrogen [2]. Considering the CO₂ emission rate, hydrogen can be the most suitable reactant to transform CO₂ into value-added chemicals. Therefore, the power-to-gas (P2G) concept has been developed in which the captured CO₂ can be transformed into synthetic natural gas, which can be distributed through the gas grid, using hydrogen which can be produced via water electrolysis using renewable energy [3]. This P2G technology is also considered to be effective to store the surplus electricity from renewable energy with characteristics of unstable electricity generation. Additionally, CO from the biomass or organic waste gasifier can be used to produce synthetic natural gas. These CO and CO₂ methanation reactions are called the Sabatier reaction described as follows.



Since these reactions are highly exothermic, a series of adiabatic reactors with intermediate heat exchangers are required to achieve high yields of methane. In order to achieve high single-pass CO and CO₂ conversions, these reactions should be performed at low temperatures using a reactor equipped with a heat exchanger, which requires a highly active catalyst.

Until now, Ni-based catalysts have been widely used in the commercial methanation process because of their relative fair activity, low cost, and high availability compared with the noble metal catalyst [4–15]. However, the low-temperature catalytic activity of Ni-based catalysts should be further improved. In order to enhance the catalytic activity, various supports [4,10–13,16–19] and a variety of preparation methods [6–8,12,13,20–23] have been investigated to fabricate the better Ni-based catalysts. Besides, the addition of second metal as a promoter has also been attempted. Various promoters such as alkali metals (Na, K [24–27]), alkali earth metals (Mg [28–30], Ca, Ba [28]), 3d transition metals (V [19], Mn [6,12,31,32], Zn [33–35]), 4d

* Corresponding author.

E-mail address: edpark@ajou.ac.kr (E.D. Park).

<https://doi.org/10.1016/j.cattod.2019.08.058>

Received 27 May 2019; Received in revised form 27 August 2019; Accepted 29 August 2019

0920-5861/© 2019 Elsevier B.V. All rights reserved.

Table 1
Physicochemical properties of Ni-based catalysts.^a

Catalyst	S_{BET}^b (m^2/g)	Pore volume ^b (cm^3/g)	Average pore diameter ^b (nm)	Ni dispersion ^c (%)	CASA ^c ($\text{m}^2/\text{g}_{\text{cat}}$)	H_2 uptake ^d ($\text{mmol}/\text{g}_{\text{cat}}$)	CO_2 uptake ^e ($\mu\text{mol}/\text{g}_{\text{cat}}$)
Ni/Al@Al ₂ O ₃ [41]	115	0.15	5.3	3.2	2.2	0.24	31
Ni-Mn/Al@Al ₂ O ₃	107	0.14	5.1	3.7	2.5	0.69	35
Ni-Zr/Al@Al ₂ O ₃	109	0.14	5.0	3.3	2.2	0.37	31
Ni-Ce/Al@Al ₂ O ₃	110	0.15	5.3	3.6	2.4	0.55	35
Ni-Mg/Al@Al ₂ O ₃	109	0.14	5.1	3.5	2.3	0.45	37
Ni-K/Al@Al ₂ O ₃	124	0.16	5.2	2.2	1.5	0.17	35
Ni-Zn/Al@Al ₂ O ₃	104	0.13	4.9	2.7	1.8	0.20	24
Ni-V/Al@Al ₂ O ₃	100	0.13	5.1	4.1	2.7	0.89	19
Ni/ γ -Al ₂ O ₃ [8]	130	0.22	7.4	1.7	1.2	0.14	28
Ni-Mn/ γ -Al ₂ O ₃	125	0.20	6.5	2.3	1.6	0.19	32
Ni-Zr/ γ -Al ₂ O ₃	112	0.19	6.8	1.8	1.2	0.14	30
Ni-Ce/ γ -Al ₂ O ₃	109	0.19	7.0	2.2	1.5	0.17	32

^a All the catalysts were calcined in the air and reduced in H₂ both at 500 °C.

^b The specific surface area, pore volume, and average pore diameter were determined by N₂ physisorption.

^c The Ni dispersion and catalytic active surface area (CASA) were determined based on the H₂ chemisorption.

^d H₂ uptake in the temperature range of 35–500 °C were determined based on the H₂-TPR.

^e The chemisorbed CO₂ uptake was measured at 35 °C.

transition metals (Zr [28,36]) and lanthanides (La [24,26], Ce [14,37–39]) were examined. However, a systematic approach is still required to find out the effect of each promoter on the catalytic activity for CO and CO₂ methanation.

Recently, we reported that the core-shell Al@Al₂O₃ provided superior heat conductivity and surface properties as a potential heterogeneous catalyst substrate for highly exothermic and endothermic reactions [40–43]. In this study, a series of promoters including Mn, Zr, Ce, Mg, K, Zn and V were incorporated into Ni/Al@Al₂O₃ and Ni/ γ -Al₂O₃ catalysts. The promoter content was fixed to be 0.5 wt.% because the addition of large amounts of the promoter was reported to result in a decrease in catalytic activity because of the blockage of the active site [25,26]. These catalysts were applied to CO and CO₂ methanation to find out the effect of each promoter on the catalytic activity. These catalysts were also characterized to find out the relationship between the catalytic activity and the physicochemical properties.

2. Experimental

2.1. Catalyst preparation

The Al@Al₂O₃ support was prepared as described in the supporting information. For comparison, γ -Al₂O₃ (neutral, Alfa Aesar) was also used as a support as received. Ni/Al@Al₂O₃ and Ni/ γ -Al₂O₃ were prepared by wet impregnation method as described previously [4]. Metal (M)-promoted Ni catalysts were prepared by co-impregnation method from an aqueous solution of Ni(NO₃)₂·6H₂O (Junsei Chemical Co., Ltd.) and precursor of a promoter such as Mn(NO₃)₂·4H₂O (Aldrich), ZrO(NO₃)₂·2H₂O (Kanto Chemical Co., Ltd.), Ce(NO₃)₃·6H₂O (Kanto Chemical Co., Ltd.), Mg(NO₃)₂·6H₂O (Kanto Chemical Co., Ltd.), KNO₃ (Daejung Chemicals & Metals Co., Ltd.), Zn(NO₃)₂·6H₂O (Daejung Chemicals & Metals Co., Ltd.), NH₄VO₃ (Aldrich), and Ni(NO₃)₂·6H₂O (Junsei Chemical Co., Ltd.). After impregnation, all samples were collected, dried in an oven at 110 °C overnight and then calcined in air at 500 °C for 3 h. The Ni and M content in supported Ni-M catalyst were intended to be 10 wt.% and 0.5 wt.%, respectively.

2.2. Catalytic activity test

The CO and CO₂ methanation were carried out in a fixed-bed quartz reactor at atmospheric pressure in the reaction temperature range of 140–450 °C as described previously [4]. 0.10 g of the catalyst (45–80 mesh) was reduced at 500 °C for 1 h in a hydrogen stream with a flow rate of 30 mL/min before being contacted with the 100 mL/min feed

gas composed of 1 mol% CO (or CO₂), 50 mol% H₂, and 49 mol% He.

The kinetic experiments were also performed separately under different reaction conditions as described in the supporting information.

The exit gas composition is analyzed using a gas chromatograph (YL Instrument 6100GC) as described in the supporting information. CO conversion, CO₂ conversion, CO yield, and C₁-C₃ hydrocarbon yield are calculated as described in the supporting information.

2.3. Characterization of catalysts

The prepared catalysts were characterized with various techniques such as N₂ physisorption, CO₂ chemisorption, H₂ chemisorption, temperature-programmed reduction with H₂ (H₂-TPR), temperature-programmed desorption of CO₂ (CO₂-TPD), X-ray diffraction (XRD), high-resolution transmission electron microscopy (HRTEM), X-ray photoelectron spectroscopy (XPS), and in-situ diffuse reflectance infrared Fourier transform spectroscopy (DRIFTS). The detailed procedure for each technique is described in the supporting information.

3. Results and discussion

3.1. Characterizations of the catalysts

The specific surface area (S_{BET}), average pore volume, and average pore diameter of supported Ni catalysts were determined by N₂ physisorption and are listed in Table 1. All Ni catalysts supported on Al@Al₂O₃ show type IIb isotherms [44], as shown in Fig. S1. The addition of a promoter does not affect significantly the textural properties of the supported Ni catalysts. The specific surface areas and pore volumes of the promoted Ni catalysts (except for Ni-K/Al@Al₂O₃ catalyst) were found to be slightly lower than those of the corresponding Ni/Al@Al₂O₃ catalyst. This is quite reasonable because the additional promoter can be dispersed throughout the pores inside the catalyst. However, the addition of K resulted in the similar S_{BET} and pore volume with Ni/Al@Al₂O₃ within the experimental error. The addition of metal precursors can affect the further oxidation of the core Al metal in Al@Al₂O₃ support resulting in the different fraction of Al core and Al₂O₃ layer in the final catalyst as listed in Table S1.

H₂ chemisorption was performed to determine the Ni dispersion and the catalytically active surface area (CASA) of all catalysts. As listed in Table 1, the noticeable improvement in Ni dispersion, as well as CASA, is observed for Ni-Mn/Al@Al₂O₃ and Ni-Mn/ γ -Al₂O₃ catalysts compared to Ni/Al@Al₂O₃ and Ni/ γ -Al₂O₃, respectively. Note that Ni/Al@Al₂O₃ has much larger CASA than Ni/ γ -Al₂O₃ and that a further

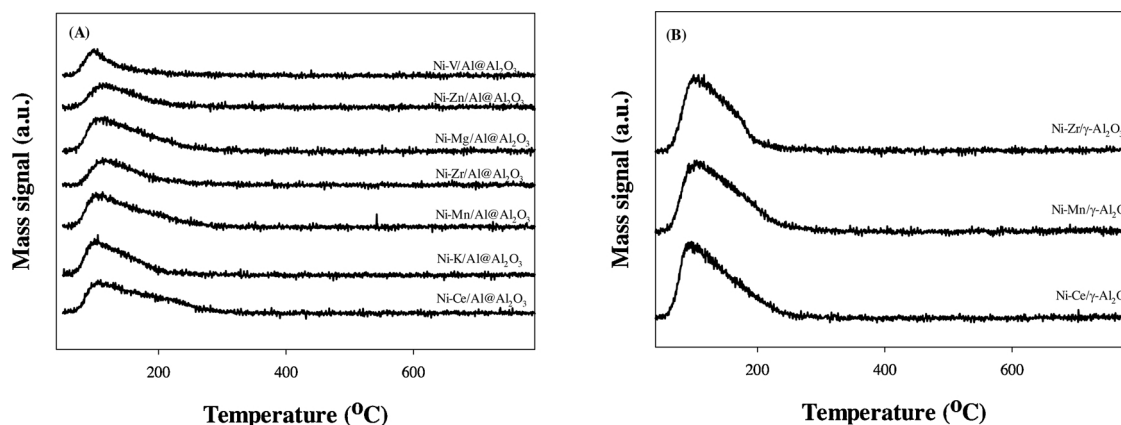


Fig. 1. CO₂-TPD patterns of Ni-based catalysts (A) supported by Al@Al₂O₃, and (B) supported by γ -Al₂O₃.

increase in CASA is achieved by the introduction of Mn to Ni/Al@Al₂O₃ catalyst. There was no noticeable change in CASA and Ni dispersion for Zr-promoted Ni/Al@Al₂O₃ catalysts, while V-, Mn-, Ce-, and Mg-promoted increasing the CASA compared with those of Ni/Al@Al₂O₃. Notably, among prepared Al@Al₂O₃-supported Ni catalysts, Ni-V/Al@Al₂O₃ shows the largest CASA and Ni dispersion. Noticeable decrease in CASA and Ni dispersion was observed for Ni-Zn/Al@Al₂O₃ and Ni-K/Al@Al₂O₃. In the case of γ -Al₂O₃-supported Ni catalysts, the CASA and Ni dispersion decreased in the following order: Ni-Mn/ γ -Al₂O₃ > Ni-Ce/ γ -Al₂O₃ > Ni-Zr/ γ -Al₂O₃ ~ Ni/ γ -Al₂O₃. The strong interaction between Ni and K or Zn was reported to cause the small CASA by blocking the surface Ni site in the case of K- or Zn-promoted Ni catalysts [26,27,35,45].

In order to assess the surface basicity of the prepared catalysts, CO₂ chemisorption and CO₂-TPD were carried out to measure the number of basic surface sites and the strengths of the basic sites, respectively. As presented in Table 1, the amounts of chemisorbed CO₂ were dependent on the promoter. Irrespective of support, Mg-promoted Ni catalysts show the largest CO₂ uptake at room temperature. The CO₂ uptake for Al@Al₂O₃-supported Ni catalysts decreased in the following order: Ni-Mg/Al@Al₂O₃ > Ni-Mn/Al@Al₂O₃ ~ Ni-Ce/Al@Al₂O₃ ~ Ni-K/Al@Al₂O₃ > Ni-Zr/Al@Al₂O₃ ~ Ni/Al@Al₂O₃ > Ni-Zn/Al@Al₂O₃ > Ni-V/Al@Al₂O₃. Note that the addition of Zn or V decreased the CO₂ uptake significantly. Fig. 1A reveals that most CO₂ molecules adsorbed onto the catalyst are desorbed at ~100 °C only except for Ni-Ce/Al@Al₂O₃, which indicates that most CO₂ molecules are adsorbed on weak basic sites [5,9]. The CO₂ desorption peaks of Ni-Ce/Al@Al₂O₃, Ni-Mn/Al@Al₂O₃, and Ni-Mg/Al@Al₂O₃ shift to the

higher temperature than that of Ni/Al@Al₂O₃, which implies that the additional moderate basic sites which are favorable for the activation of CO₂ are formed over them [6,7,10,17,46]. Fig. 1B reveals that similar CO₂-TPD patterns with those of Al@Al₂O₃-supported Ni catalysts were obtained for all Ni catalysts supported on γ -Al₂O₃, wherein a TPD peak for each catalyst appeared at ~100 °C.

The XRD patterns of reduced samples are shown in Fig. 2 to confirm any changes in the composition when the promoter was added to supported Ni catalysts. Fig. 2A confirms that the core-shell structure of Al@Al₂O₃ support remains after the co-impregnation of Ni and promoter by the detection of Al (JCPDS 04-0787) and γ -Al₂O₃ (JCPDS 29-0063). The crystallite size of the metallic Ni in the reduced catalyst supported on Al@Al₂O₃ cannot be calculated because of the peak overlap due to Ni and Al. In the case of Ni-based catalysts supported on γ -Al₂O₃, the XRD peaks due to Ni (JCPDS 04-0850) are observed in Fig. 2B indicating the transformation of NiO into Ni during the reduction process. Compared with those of Ni/ γ -Al₂O₃ [8], rather broad XRD peaks due to the metallic Ni were observed for Mn-, Ce-, and Zr-promoted Ni/ γ -Al₂O₃ catalysts indicating that these promoters increased the Ni dispersion. The smallest crystallite size of Ni was obtained for Ni-Mn/ γ -Al₂O₃ catalyst among γ -Al₂O₃-supported Ni catalysts. Moreover, the decrease in the Al core fraction was observed in the promoted Ni-M/Al@Al₂O₃ (Table S1), implying that the core Al was further transformed into Al₂O₃ during its preparation for this catalyst.

Fig. 3 shows the H₂-TPR profiles of the Ni-based catalysts calcined at 500 °C. The H₂ uptake of each catalyst calculated based on H₂-TPR profiles in the temperature range of 35–500 °C is presented in Table 1. In Fig. 3A, the low-temperature TPR peak is observed for all samples

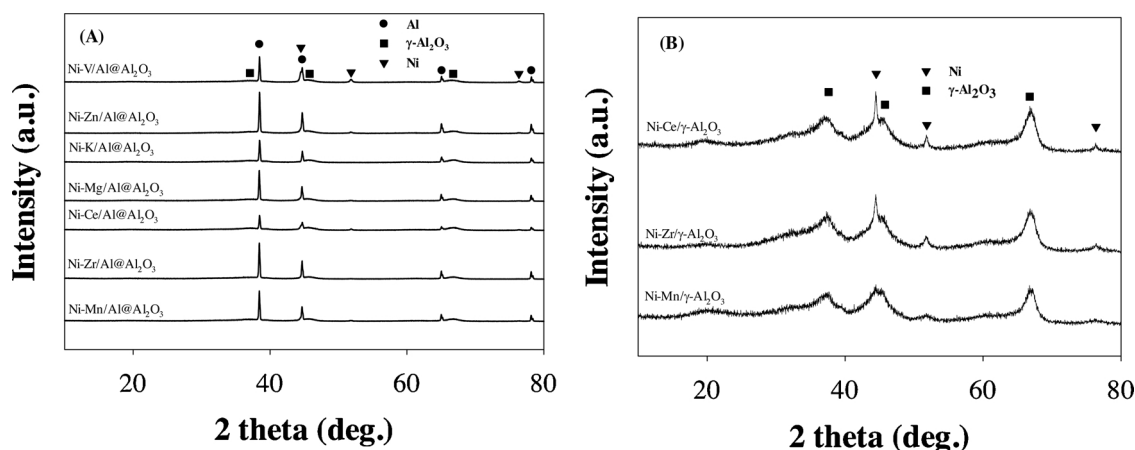


Fig. 2. XRD patterns of reduced Ni catalysts (A) supported by Al@Al₂O₃, and (B) supported by γ -Al₂O₃. (●) Al JCPDS 04-0787, (▼) Ni JCPDS 04-0850, and (■) γ -Al₂O₃ JCPDS 29-0063.

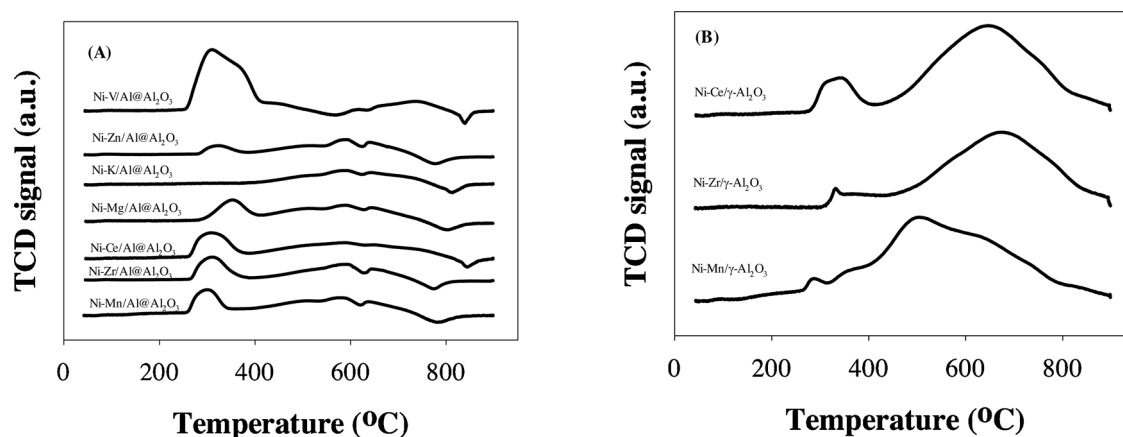


Fig. 3. H₂-TPR profiles of Ni-based catalysts calcined at 500 °C; (A) supported by Al@Al₂O₃, and (B) supported by γ -Al₂O₃.

only except for Ni-K/Al@Al₂O₃ in the temperature range of 260–310 °C, which implies the presence of NiO interacting weakly with the support. In the case of Ni-V/Al@Al₂O₃, this low-temperature TPR peak can also be assigned to the reduction of some V-containing phase [47]. The TPR peaks at high temperatures (400–500 °C) indicate the reduction of NiO species interacting strongly with the support. A small negative TPR peak at ~ 600 °C is attributed to the physical melting of Al core. The H₂ uptake of Ni-Mn/Al@Al₂O₃ is larger than the others only except for Ni-V/Al@Al₂O₃. Similarly, the low-temperature TPR peaks are observed for Mn-, Zr-, and Ce-promoted Ni/ γ -Al₂O₃ samples, as shown in Fig. 3B. The highest H₂ consumption (0.19 mmol/g_{cat.}) was obtained for Ni-Mn/ γ -Al₂O₃. Ni/Al@Al₂O₃ [41] and Ni/ γ -Al₂O₃ [8] show the only high-temperature TPR peak with a peak maximum at above 500 °C indicating the low reduction degree of nickel oxides when the catalyst was reduced at 500 °C. Consequently, the addition of promoters such as Mn, Zr, Ce, Mg, and V can improve the reducibility of NiO resulting in higher reduction degree of NiO and possibly higher catalytic activity than the unpromoted supported Ni catalysts. On the other hand, K- or Zn-promoted Ni/Al@Al₂O₃ samples have lower H₂ uptakes than the Ni/Al@Al₂O₃ sample, which implies that the former catalysts would have lower reduction degree of NiO than the latter catalyst when they are reduced at 500 °C. This is responsible for their low Ni dispersions, CASAs, and catalytic activity for CO and CO₂ methanation.

Fig. 4A illustrates the HRTEM image of the Ni-Mn/Al@Al₂O₃ catalyst. There is a rather uniform particle size distribution of Ni metal. The average particle size of Ni metal is determined to be around 5 nm (Fig. 4B). The typical STEM dark field image and corresponding elemental maps (Fig. 4C) confirm that Mn, Ni, Al, and O elements are well distributed in the Ni-Mn/Al@Al₂O₃ catalyst.

X-ray photoelectron spectroscopy (XPS) studies were carried out on Ni-Mn/Al@Al₂O₃ and Ni-Mn/ γ -Al₂O₃ samples with to determine the oxidation state of the metals and the surface composition in the reduced state. The bands observed at 851–852 and 854–856 eV (Fig. 5B) can be assigned as Ni 2p_{3/2} XPS spectra corresponding to the metallic Ni [48] and nickel oxide/hydroxide [49,50], respectively. The above results indicated that Ni species existed as Ni⁰ and NiO. Note that the fraction of the metallic Ni in Ni-Mn/Al@Al₂O₃ was higher than those in Ni-Mn/ γ -Al₂O₃ and Ni/Al@Al₂O₃ (Table S2). This is consistent with the fact that Ni-Mn/Al@Al₂O₃ has a higher H₂ uptake than Ni-Mn/ γ -Al₂O₃ and Ni/Al@Al₂O₃ during H₂-TPR (Table 1). The Ni 2p_{3/2} XPS spectra obtained for Ni/Al@Al₂O₃, Ni-K/Al@Al₂O₃, and Ni-Zn/Al@Al₂O₃ confirm that the fraction of the metallic Ni was decreased when K or Zn was added as a promoter (Fig. S2). This is also consistent with the result that Ni-K/Al@Al₂O₃ and Ni-Zn/Al@Al₂O₃ have lower H₂ uptake during H₂-TPR than Ni/Al@Al₂O₃ (Table 1). From the spectra of Fig. 5C, Mn(II), Mn(III), and Mn(IV) species are confirmed to coexist because the corresponding XPS spectra were found in the range of 630–650 eV [51].

Each fraction was also quantified and listed in Table S2. Similar distribution of Mn(II), Mn(III), and Mn(IV) species are confirmed for both Ni-Mn/ γ -Al₂O₃ and Ni-Mn/Al@Al₂O₃.

3.2. CO methanation

The catalytic activity for CO methanation over Al@Al₂O₃-supported Ni catalysts was obtained and displayed in Fig. 6A. The addition of V, Mn, Ce, Mg, and Zr into Ni/Al@Al₂O₃ improved the catalytic performance for CO methanation. Note that these catalysts have higher H₂ uptakes determined by H₂-TPR and higher Ni dispersion as well as CASA calculated based on H₂ chemisorption. On the other hand, the negative effect on CO methanation was observed over Zn-, and K-doped Ni/Al@Al₂O₃ catalysts which can be due to the significant decrease of CASA (Table 1). In terms of product yield, methane is a predominant product at all reaction temperatures, while ethane and propane are also detected as byproducts (Fig. S3).

The Arrhenius plots for CH₄ formation rate for CO methanation over Al@Al₂O₃-supported Ni catalysts (Fig. 6B) provide the activation energies (E_a) in the range of 93–120 kJ/mol (Table 2). The most active catalyst (Ni-V/Al@Al₂O₃) shows the highest CH₄ formation rate of 0.242 mol·h⁻¹·g⁻¹ at 200 °C with the low apparent E_a of 96 kJ/mol among tested catalysts.

The improvement of the CO methanation activity was also observed over Mn-, Ce-, and Zr-promoted Ni/ γ -Al₂O₃ catalysts (Fig. S4), which is consistent with the previous reports [6,12,15,31,32,34,36,37,39,52,53]. The CO methanation activity is dependent on the surface area of the metallic Ni, which affects the CO activation and dissociation and the production of highly active surface H species. The enhanced catalytic activity of promoted Ni catalysts was reported to be related to the improvement of Ni dispersion [5]. The Ce-doped Ni/ γ -Al₂O₃ catalyst was reported to promote CO methanation due to high Ni dispersion [37,38]. Hu et al. [26] demonstrated that the addition of Zr, Co, Ce, Zn, and La possessed high catalytic activity for CH₄ formation and good catalytic stability, which were attributed to the formation of smaller Ni nanoparticles with high metal dispersion. Zr promoter was also reported to be able to produce oxygen vacancies, thereby increasing the ability of CO to adsorb and dissociate [36]. Zr promoter was also claimed as the best promoter among Zr, Mg, Ba, and Ca to enhance coking resistance by reducing the rate of polymeric carbon formation through CO methanation [28]. 2–4 wt% of MgO adding to Ni/Al₂O₃ was reported to enhance the CO methanation activity via the small NiO particles formation and improve the catalytic stability by reducing the carbon deposition [29]. MnO_x promoter was reported to restrain the sintering and aggregation of Ni due to the formation of relatively small Ni nanoparticles and to provide more oxygen vacancies, which is conducive to the removal of carbonaceous species for anti-coking [12].

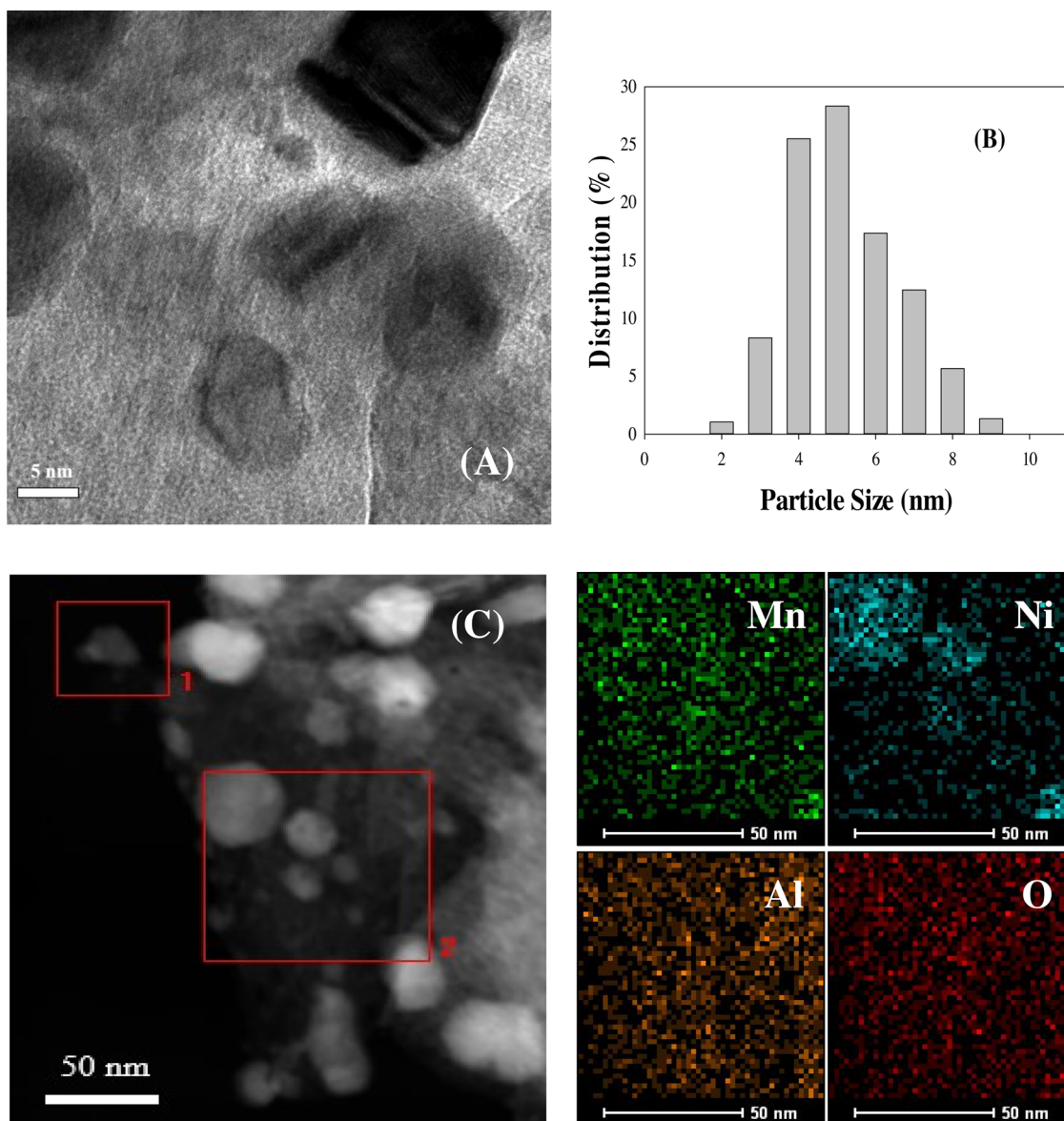


Fig. 4. (A) HRTEM image, (B) size distribution, and (C) elemental mapping of Ni-Mn/Al@Al₂O₃ catalyst.

In this study, the CASA was not increased noticeably when 0.5 wt% Zr was added. Therefore, it can be said that the nature of support, such as ZrO_x-Al₂O₃, might affect the CO dissociation rate, which is the intermediate step in CO methanation [34,52,54]. Moreover, it was reported that Zr was effective to reduce carbon formation [28,52]. Among tested catalysts, the V-promoted Ni catalyst is the best one because it has the largest CASA. The promotional effect of V in supported Ni-V catalyst on CO methanation is still controversial. There are some reports

in which V-promoted Ni/Al₂O₃ improved CO methanation due to its large H₂ uptake and high Ni dispersion [36,55–57]. They stated that the CO dissociation was improved by electron transferring from V species to Ni⁰. In this study, we also observed the high H₂ consumption during TPR experiment.

Zn was reported to make strong interactions with Ni, cover Ni particles, and decrease the chemisorption amount of CO, which is not favorable for the CO dissociation on Ni-Zn alloy [33]. The specific

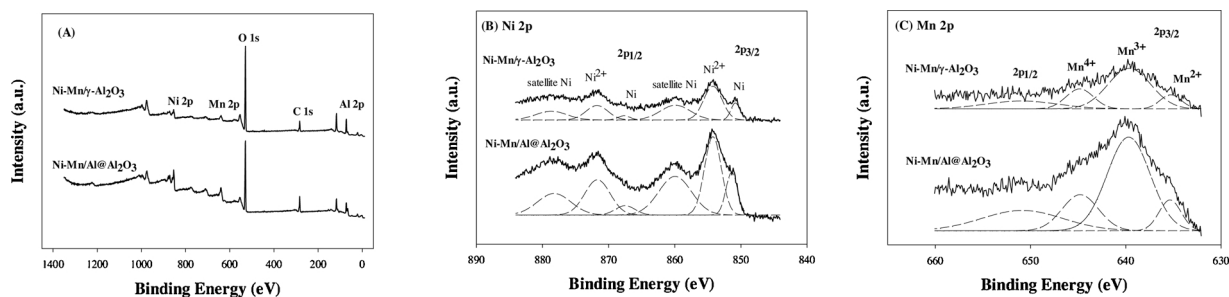


Fig. 5. XPS spectra of reduced Ni-Mn/Al@Al₂O₃ and Ni-Mn/ γ -Al₂O₃ catalysts; (A) full scan, (B) Ni 2p, and (C) Mn 2p.

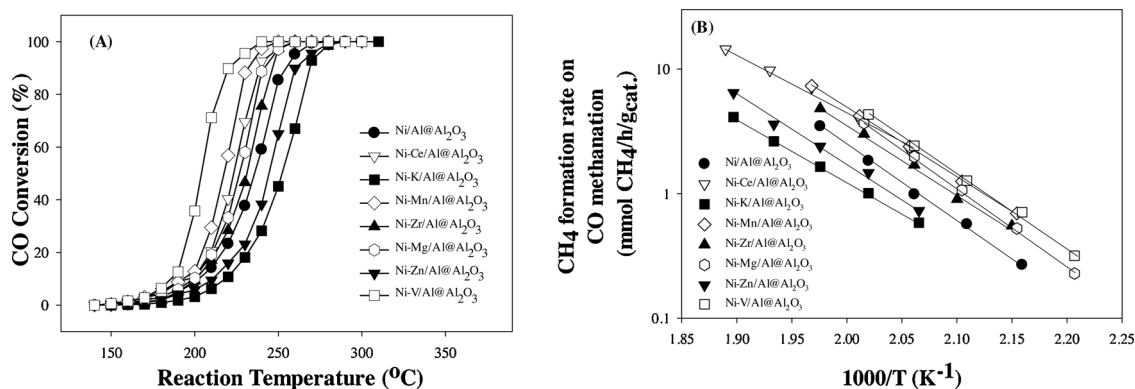


Fig. 6. Catalytic performance of Ni-based catalysts supported by Al@Al₂O₃ for CO methanation; (A) CO conversion, and (B) CH₄ formation rate. All the catalysts were calcined in air at 500 °C and reduced by H₂ at 500 °C. Reaction conditions: 1 mol% CO, 50 mol% H₂, 49 mol% He, F/W = 1000 mL/min/g_{cat}. The data for Ni/Al@Al₂O₃ [41] are included for easy comparison.

Table 2

Activity comparison for CO and CO₂ methanation among Ni-based catalysts.

Catalyst	CO Methanation		CO ₂ Methanation	
	E _a (kJ/mol)	Specific reaction rate at 200 °C (mol CH ₄ ·h ⁻¹ ·g ⁻¹)	E _a (kJ/mol)	Specific reaction rate at 220 °C (mol CH ₄ ·h ⁻¹ ·g ⁻¹)
Ni/Al@Al ₂ O ₃ [41]	115	0.099	83	0.219
Ni-Mn/Al@Al ₂ O ₃	106	0.239	82	0.462
Ni-Ce/Al@Al ₂ O ₃	93	0.225	76	0.332
Ni-Zr/Al@Al ₂ O ₃	106	0.170	68	0.263
Ni-Mg/Al@Al ₂ O ₃	120	0.198	82	0.320
Ni-Zn/Al@Al ₂ O ₃	103	0.073	80	0.162
Ni-K/Al@Al ₂ O ₃	114	0.058	83	0.185
Ni-V/Al@Al ₂ O ₃	96	0.242	74	0.280

amount of K was reported to inhibit methane formation [26]. ZnO is more reactive towards CO than CeO₂ [33], and the strong interaction between Ni and ZnO led to the CH₄ suppression in CO methanation [35]. A small amount of alkali metal such as Na and K was reported to improve the CO methanation performance by increasing the metal dispersion [25,26]. Conversely, promotional effects were not always positive; for instance, using K can inhibit the CH₄ formation in Ni-K/Al₂O₃ [26,27], and increase the selectivity of undesired higher hydrocarbons in products as a consequence of direct K-Ni interactions [27].

3.3. CO₂ methanation

The catalytic activity for CO₂ methanation was measured over the Al@Al₂O₃-supported Ni catalysts. As shown in Fig. 7A, Ni-Mn/Al@Al₂O₃ shows the highest catalytic activity for CO₂ methanation among the tested catalysts. This result is related to the combination of the high CASA, high CO₂ uptake capacity, and moderate binding strength of CO₂ by the introduction of Mn promoter. High CASA supplies high surface H concentration for the hydrogenation of intermediates species is the rate-determining step [5,8,20], and the high CO₂ uptake capacity coupled with strong interactions with catalyst surface promotes the high catalytic activity for CO₂ methanation [6,9,20,58]. Interestingly, Ni-V/Al@Al₂O₃ with a higher Ni dispersion but smaller CO₂ uptake shows the higher catalytic activity for CO₂ methanation than Ni/Al@Al₂O₃, while Ni-K/Al@Al₂O₃ with a lower Ni dispersion but higher CO₂ uptake obtains the lower activity. This result reveals the synergic effect between Ni dispersion and CO₂ uptake in CO₂ methanation. Methane was a major product during CO₂ methanation (Fig. S5). The formation of C₂H₆ was observed over Ni-Ce/Al@Al₂O₃ and Ni/Al@Al₂O₃ catalysts. CO formation via reverse water gas shift (RWGS) reaction was confirmed over Ni(-K, -Mg, -Zn, -V)/Al@Al₂O₃ catalyst. These promoters could promote the RWGS reaction. The beneficial effect of Mn, Ce, and Zr in promoted Ni catalysts supported on γ-Al₂O₃ on CO₂ methanation was also observed (Fig. S6). The catalytic activity for CO₂ methanation decreased in the following order: Ni-Mn/γ-Al₂O₃ > Ni-Ce/γ-Al₂O₃ > Ni-Zr/γ-Al₂O₃ > Ni/γ-Al₂O₃.

The Arrhenius plots for the CH₄ formation rate during CO₂ methanation displayed in Fig. 7B confirm the trend observed in Fig. 7A. The CH₄ formation rate decreased in the following order: Ni-Mn/

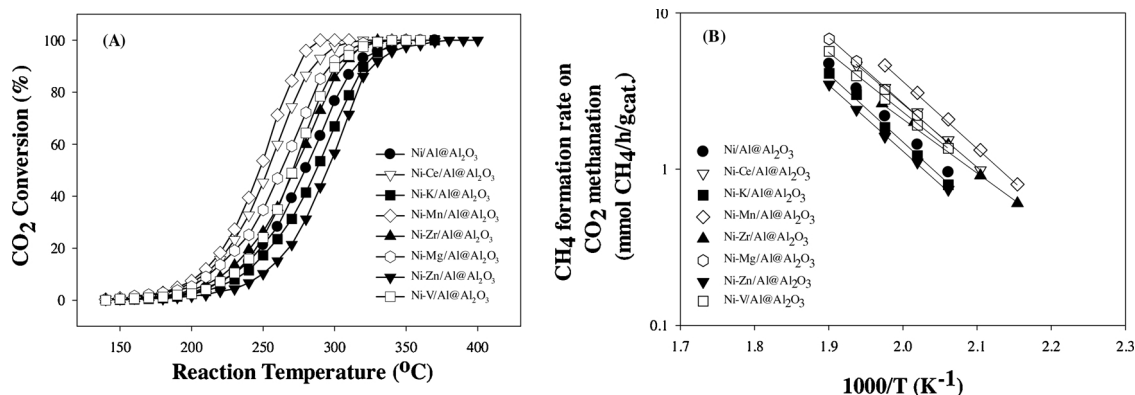


Fig. 7. Catalytic performance of Ni-based catalysts supported by Al@Al₂O₃ for CO₂ methanation; (A) CO₂ conversion, and (B) CH₄ formation rate. All the catalysts were calcined in air at 500 °C and reduced by H₂ at 500 °C. Reaction conditions: 1 mol% CO₂, 50 mol% H₂, 49 mol% He, F/W = 1000 mL/min/g_{cat}. The data for Ni/Al@Al₂O₃ [41] are included for easy comparison.

Al@Al₂O₃ > Ni-Ce/Al@Al₂O₃ > Ni-Mg/Al@Al₂O₃ > Ni-V/Al@Al₂O₃ ~ Ni-Zr/Al@Al₂O₃ > Ni/Al@Al₂O₃ > Ni-K/Al@Al₂O₃ > Ni-Zn/Al@Al₂O₃. The apparent E_a of all catalysts in the kinetic experiment for CO₂ methanation were found to be in the range of 68–83 kJ/mol as listed in Table 2.

Ni/γ-Al₂O₃ catalysts doped with Ce was reported to enhance the CO₂ methanation performance thanks to the possible activation of CO₂ [14,39]. Hu et al. [26] demonstrated that the addition of Zr, Co, Ce, Zn, and La possessed high catalytic activity for CH₄ formation and good catalytic stability, which were attributed to the formation of smaller Ni nanoparticles with high metal dispersion. Mg was reported to be a potential promoter for CO₂ methanation by improving the Ni dispersion, as well as the active CO₂ amount over Ni-Mg-USY zeolite catalysts [30]. La, K, and Na were proposed to increase CO₂ methanation activity in the coexistence of CO and CO₂ condition [24]. The active sites that are responsible for CO₂ methanation reaction were proposed as the basic metallic surface centers and oxygen vacancy sites [59].

3.4. In-situ DRIFTS analysis

In-situ DRIFTS experiments were performed to study the evolution of surface species during CO₂ methanation over the most active Ni-Mn/Al@Al₂O₃ catalyst. Fig. S7 shows the infrared spectra of the surface species formed on this catalyst after the adsorption of CO₂ at different temperatures for 20 min in order to probe the surface basicity of these catalysts. Three kinds of basic sites distinguished on the catalyst can be classified as bicarbonate (at $\nu = 1650\text{ cm}^{-1}$, $\nu = 1440\text{ cm}^{-1}$ and $\nu = 1230\text{ cm}^{-1}$), monodentate carbonate ($\nu = 1390\text{ cm}^{-1}$ and $\nu = 1530\text{ cm}^{-1}$), and bidentate carbonate ($\nu = 1590\text{ cm}^{-1}$ and $\nu = 1320\text{ cm}^{-1}$) [6,46,60–63]. The band intensity at 1650, 1440, and 1230 cm⁻¹ corresponding to the weak bicarbonate decreased significantly with increasing temperature. On the other hand, the bands due to monodentate carbonate and bidentate carbonate were weakened a little after increasing temperature up to 300 °C. Each band corresponding to a different basic site was deconvoluted and quantified in Table S3. Compared with Ni/γ-Al₂O₃ and Ni/Al@Al₂O₃ catalysts [41], the fraction of moderate basic sites forming bidentate carbonate species is predominantly found over Ni-Mn/Al@Al₂O₃. On the other hand, the fraction of weak basic sites forming bicarbonate species decreased in the following order: Ni/γ-Al₂O₃ (55.5%) > Ni/Al@Al₂O₃ (46.3%) > Ni-Mn/Al@Al₂O₃ (28.7%). Considering the largest CO₂ uptake capacity of Ni-Mn/Al@Al₂O₃ (Table 1), we can say that this catalyst is confirmed to possess the higher density of medium and strong basic sites than Ni/Al@Al₂O₃ and Ni/γ-Al₂O₃. This is beneficial for higher catalytic activity for CO₂ methanation.

Fig. 8 shows the formation of various surface intermediates during CO₂ hydrogenation at different temperatures from 150 °C to 300 °C.

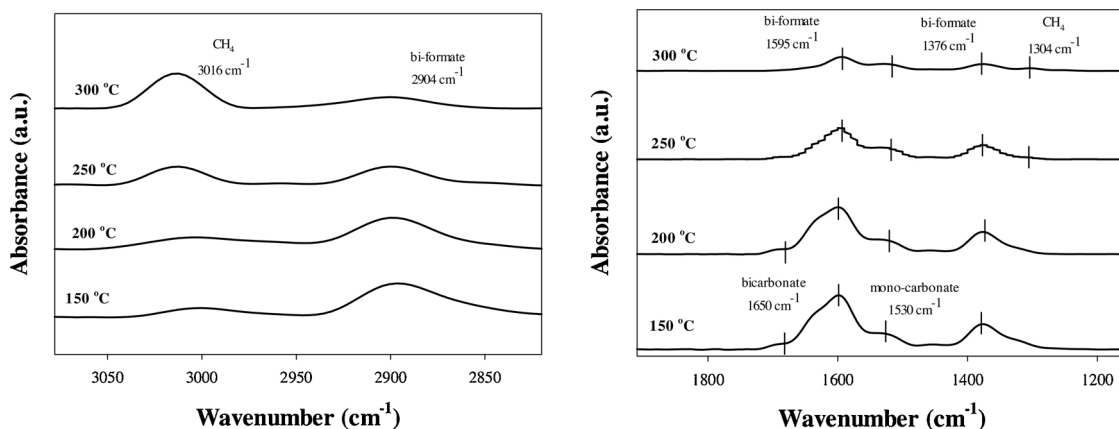


Fig. 8. In situ DRIFTS spectra over Ni-Mn/Al@Al₂O₃ observed during CO₂ methanation from 150 to 300 °C. The catalyst was contacted with the feed gas composed of 1 mol% CO₂, 50 mol% H₂, and 49 mol% He with a total flow of 50 mL/min.

Immediate appearance of new bands at 3016, 2904, 1595, 1376, and 1304 cm⁻¹ was observed with accompanying apparent attenuation of the carbonates bands at 1650 and 1530 cm⁻¹ at low reaction temperatures. The disappearance of peaks at 1590, 1440, 1390, 1320 and 1230 cm⁻¹ can be explained by the transformation of carbonates species into intermediates during CO₂ hydrogenation. The new peaks can be classified into two groups: (i) 2904, 1595 and 1376 cm⁻¹, and (ii) 3016 and 1304 cm⁻¹. The former and the latter group can be assigned to bidentate formate species and methane, respectively [6,7,16,17,58,64,65]. With increasing reaction temperature, the fraction ratio of formate species to carbonates species reached a maximum at 300 °C with the continuous consumption of carbonates, suggesting a transformation of carbonates into formate species with the steady supply of H₂ [7]. The peak intensity of formate species decreased along with the continuous formation of surface methane species. According to the IR data, we can conclude that CO₂ methanation over Ni-Mn/Al@Al₂O₃ proceeds with the initial formation of carbonates due to CO₂ adsorption, their hydrogenation into formate species, and finally subsequent transformation into methane. There are two main different mechanisms on CO₂ methanation. One is that the process might involve the conversion of CO₂ to CO before being hydrogenated to methane [64,66,67]. The other involves the direct hydrogenation of CO₂ to methane without forming a CO intermediate [11,46,58,59,65,67]. Based on the IR study, it can be said that direct hydrogenation of CO₂ proceeds over Ni-Mn/Al@Al₂O₃ catalysts.

3.5. Stability

In order to evaluate the stability of the most active catalysts (Ni-Mn/Al@Al₂O₃ and Ni-Mn/γ-Al₂O₃) during CO and CO₂ methanation, the long-term stability test was carried out. As shown in Fig. 9, CO and CO₂ conversion were maintained over these two catalysts for 50 h. The bulk crystalline structure is confirmed not to be changed by XRD analysis for the catalyst before and after the stability test (Fig. S8). No detectable signal was found due to crystalline carbon (graphite and whisker carbon) or NiO. There is no change in the intensity ratio of peaks due to Al and Al₂O₃ for the Ni-Mn/Al@Al₂O₃ after the stability test, which indicates that the core-shell structure of Al@Al₂O₃ support is maintained.

4. Conclusion

The catalytic activity for CO and CO₂ methanation was strongly dependent on the kind of promoter (M = Mn, Ce, Zr, Mg, K, Zn, or V) in Ni-M/Al@Al₂O₃ catalysts. Mn, Ce, Mg, V, and Zr have a positive effect on both reactions. On the other hand, K and Zn have a negative effect on both reactions. The Ni dispersion and CASA are critical factors to

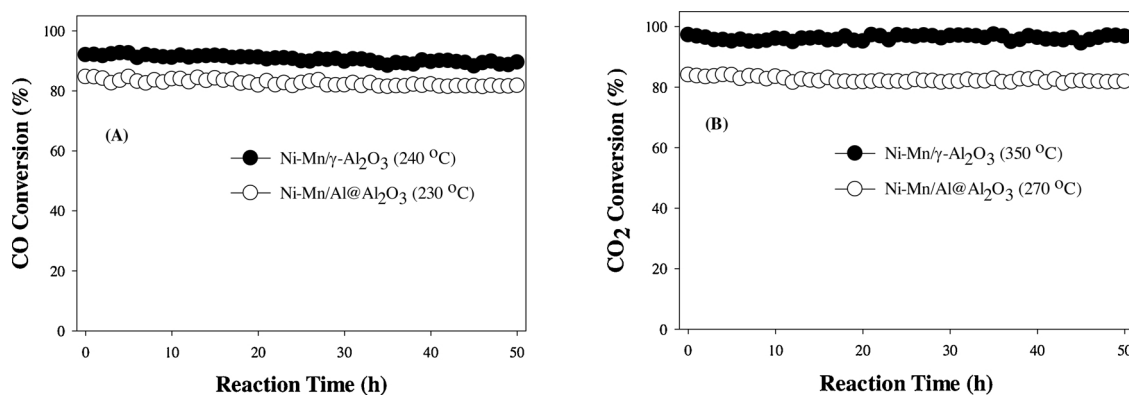


Fig. 9. Stability test over Ni-Mn/γ-Al₂O₃ and Ni-Mn/Al@Al₂O₃ for (A) CO methanation, and (B) CO₂ methanation during 50 h. Reaction conditions for CO and CO₂ methanation were the same as those in Figs. 6 and 7, respectively.

affect the catalytic activity for CO methanation. Besides them, CO₂ uptake and moderate binding strength of chemisorbed CO₂ are further required to guarantee the high catalytic activity for CO₂ methanation. The most positive effect of Mn promoter for both CO and CO₂ methanation was also confirmed in Ni-Mn/Al@Al₂O₃ catalysts. The direct hydrogenation of surface carbonate species seems to be the main pathway for CO₂ methanation over Ni-Mn/Al@Al₂O₃ catalyst. The catalytic stability for methanation process is guaranteed over Ni-Mn/Al@Al₂O₃ and Ni-Mn/γ-Al₂O₃ for 50 h.

Acknowledgments

This work was supported by the Human Resources Program in Energy Technology (No. 20154010200820) of the Korea Institute of Energy Technology Evaluation and Planning (KETEP), which is granted financial resources from the Ministry of Trade, Industry, and Energy of the Republic of Korea. This work was also supported by the Basic Science Research Program through the National Research Foundation of Korea (NRF) funded by the Ministry of Science and ICT (2017R1A2B3011316).

Appendix A. Supplementary data

Supplementary material related to this article can be found, in the online version, at doi:<https://doi.org/10.1016/j.cattod.2019.08.058>.

References

- [1] J. Klankermayer, S. Wesselbaum, K. Beydoun, W. Leitner, *Angew. Chem. Int. Ed.* 55 (2016) 7296–7343.
- [2] T. Sakakura, J.-C. Choi, H. Yasuda, *Chem. Rev.* 107 (2007) 2365–2387.
- [3] M. Götz, J. Lefebvre, F. Mörs, A. McDaniel Koch, F. Graf, S. Bajohr, R. Reimert, T. Kolb, *Renew. Energ.* 85 (2016) 1371–1390.
- [4] T.A. Le, M.S. Kim, S.H. Lee, T.W. Kim, E.D. Park, *Catal. Today* 293–294 (2017) 89–96.
- [5] T.A. Le, T.W. Kim, S.H. Lee, E.D. Park, *Korean J. Chem. Eng.* 34 (2017) 3085–3091.
- [6] T. Burger, F. Koschany, O. Thomys, K. Köhler, O. Hinrichsen, *Appl. Catal. A-Gen.* 558 (2018) 44–54.
- [7] X. Guo, Z. Peng, M. Hu, C. Zuo, A. Traitangwong, V. Meeyoo, C. Li, S. Zhang, *Ind. Eng. Chem. Res.* 57 (2018) 9102–9111.
- [8] T.A. Le, J.K. Kang, S.H. Lee, E.D. Park, *J. Nanosci. Nanotechnol.* 19 (2019) 3252–3262.
- [9] A. Vita, C. Italiano, L. Pino, P. Frontera, M. Ferraro, V. Antonucci, *Appl. Catal. B-Environ.* 226 (2018) 384–395.
- [10] T.A. Le, J.K. Kang, E.D. Park, *Top. Catal.* 61 (2018) 1537–1544.
- [11] X. Guo, A. Traitangwong, M. Hu, C. Zuo, V. Meeyoo, Z. Peng, C. Li, *Energ. Fuel.* 32 (2018) 3681–3689.
- [12] X. Lu, F. Gu, Q. Liu, J. Gao, L. Jia, G. Xu, Z. Zhong, F. Su, *Ind. Eng. Chem. Res.* 54 (2015) 12516–12524.
- [13] F. Meng, X. Li, G.M. Shaw, P.J. Smith, D.J. Morgan, M. Perdjon, Z. Li, *Ind. Eng. Chem. Res.* 57 (2018) 4798–4806.
- [14] W. Nie, X. Zou, X. Shang, X. Wang, W. Ding, X. Lu, *Fuel* 202 (2017) 135–143.
- [15] Q. Liu, J. Gao, M. Zhang, H. Li, F. Gu, G. Xu, Z. Zhong, F. Su, *RSC Adv.* 4 (2014) 16094–16103.

- [16] M.C. Bacariza, I. Graça, S.S. Bebiano, J.M. Lopes, C. Henriques, *Chem. Eng. Sci.* 175 (2018) 72–83.
- [17] Y. Yan, Y. Dai, Y. Yang, A.A. Lapkin, *Appl. Catal. B-Environ.* 237 (2018) 504–512.
- [18] M. Li, H. Amari, A.C. van Veen, *Appl. Catal. B-Environ.* 239 (2018) 27–35.
- [19] Q. Liu, F. Gu, X. Lu, Y. Liu, H. Li, Z. Zhong, G. Xu, F. Su, *Appl. Catal. A Gen.* 488 (2014) 37–47.
- [20] D. Beierlein, D. Häussermann, M. Pfeifer, T. Schwarz, K. Stöwe, Y. Traa, E. Klemm, *Appl. Catal. B-Environ.* 247 (2019) 200–219.
- [21] K. Stangeland, D. Kalai, H. Li, Z. Yu, *Energy Procedia* 105 (2017) 2022–2027.
- [22] Z. Li, L. Zhang, K. Zhao, L. Bian, *Trans. Tianjin Univ.* 24 (2018) 471–479.
- [23] C. Li, Y.-W. Chen, *Thermochim. Acta* 256 (1995) 457–465.
- [24] S. Tada, R. Kikuchi, *Catal. Sci. Technol.* 5 (2015) 3061–3070.
- [25] T.A. Le, T.W. Kim, S.H. Lee, E.D. Park, *Catal. Today* 303 (2018) 159–167.
- [26] X. Hu, G. Lu, *Green Chem.* 11 (2009) 724–732.
- [27] C.T. Campbell, D.W. Goodman, *Surf. Sci.* 123 (1982) 413–426.
- [28] J. Barrientos, N. Gonzalez, M. Boutonnet, S. Järås, *Top. Catal.* 60 (2017) 1276–1284.
- [29] D. Hu, J. Gao, Y. Ping, L. Jia, P. Gunawan, Z. Zhong, G. Xu, F. Gu, F. Su, *Ind. Eng. Chem. Res.* 51 (2012) 4875–4886.
- [30] M.C. Bacariza, I. Graça, S.S. Bebiano, J.M. Lopes, C. Henriques, *Energ. Fuel.* 31 (2017) 9776–9789.
- [31] A. Zhao, W. Ying, H. Zhang, M. Hongfang, D. Fang, *J. Nat. Gas. Chem.* 21 (2012) 170–177.
- [32] K. Zhao, Z. Li, L. Bian, *Front. Chem. Sci. Eng.* 10 (2016) 273–280.
- [33] W.G. Reimers, M.A. Baltanás, M.M. Branda, *J. Mol. Model.* 20 (2014) 2270.
- [34] Z. He, X. Wang, R. Liu, S. Gao, T. Xiao, *Appl. Petrochem. Res.* 6 (2016) 235–241.
- [35] W. Wang, X. Li, Y. Zhang, R. Zhang, H. Ge, J. Bi, M. Tang, *Catal. Sci. Technol.* 7 (2017) 4413–4421.
- [36] H. Li, J. Ren, X. Qin, Z. Qin, J. Lin, Z. Li, *RSC Adv.* 5 (2015) 96504–96517.
- [37] Y.Z. Wang, F.M. Li, H.M. Cheng, L.Y. Fan, Y.X. Zhao, *J. Fuel Chem. Technol.* 41 (2013) 972–977.
- [38] H.X. Cao, J. Zhang, C.L. Guo, J.G. Chen, X.K. Ren, *Chinese J. Catal.* 38 (2017) 1127–1137.
- [39] L. Xu, F. Wang, M. Chen, D. Nie, X. Lian, Z. Lu, H. Chen, K. Zhang, P. Ge, *Int. J. Hydrog. Energy.* 42 (2017) 15523–15539.
- [40] J. Kim, D. Lee, *Top. Catal.* 58 (2015) 375–385.
- [41] T.A. Le, J. Kim, J.K. Kang, E.D. Park, *Catal. Today* (2019), <https://doi.org/10.1016/j.cattod.2019.09.028>.
- [42] J. Kim, D. Lee, *Chem. Mater.* 28 (2016) 2786–2794.
- [43] T.A. Le, J. Kim, Y.R. Jeong, E.D. Park, *Catalysts* 9 (2019) 599–610.
- [44] F. Rouquerol, J. Rouquerol, K.S.W. Sing, G. Maurin, P. Llewellyn, 1 - introduction, in: F. Rouquerol, J. Rouquerol, K.S.W. Sing, P. Llewellyn, G. Maurin (Eds.), *Adsorption by Powders and Porous Solids (Second Edition)*, Academic Press, Oxford, 2014, pp. 1–24.
- [45] L.L. Song, Y. Yu, X.X. Wang, G.Q. Jin, Y.Y. Wang, X.Y. Guo, *Korean Chem. Eng. Res.* 52 (2014) 678–687.
- [46] Q. Pan, J. Peng, T. Sun, S. Wang, S. Wang, *Catal. Commun.* 45 (2014) 74–78.
- [47] E.V. Korneeva, T.Y. Kardash, V.A. Rogov, E.A. Smal, V.A. Sadykov, *Catal. Sustain. Energ.* 4 (2017) 17–24.
- [48] R. Wang, Y. Li, R. Shi, M. Yang, *J. Mol. Catal. A Chem.* 344 (2011) 122–127.
- [49] B.W. Hoffer, A. Dick van Langeveld, J.-P. Janssens, R.L.C. Bonn e, C.M. Lok, J.A. Moulijn, *J. Catal.* 192 (2000) 432–440.
- [50] N. Weidler, J. Schuch, F. Knaus, P. Stenner, S. Hoch, A. Maljusch, R. Sch afer, B. Kaiser, W. Jaegermann, *J. Phys. Chem. C* 121 (2017) 6455–6463.
- [51] H.W. Nesbitt, D. Banerjee, *Am. Mineral.* 83 (1998) 305–315.
- [52] Q. Liu, F. Gu, J. Gao, H. Li, G. Xu, F. Su, *J. Energy Chem.* 23 (2014) 761–770.
- [53] W. Ahmad, M.N. Younis, R. Shawabkeh, S. Ahmed, *Catal. Commun.* 100 (2017) 121–126.
- [54] M. Escobar, F. Gracia, A. Karelovic, R. Jim enez, *Catal. Sci. Technol.* 5 (2015) 4532–4541.
- [55] X. Lu, F. Gu, Q. Liu, J. Gao, Y. Liu, H. Li, L. Jia, G. Xu, Z. Zhong, F. Su, *Fuel Process. Technol.* 135 (2015) 34–46.
- [56] H.X. Cao, J. Zhang, C.L. Guo, J.G. Chen, X.K. Ren, *Appl. Surf. Sci.* 426 (2017)

- 40–49.
- [57] Z.J. Zhao, T. Wu, C. Xiong, G. Sun, R. Mu, L. Zeng, J. Gong, *Angew. Chem. Int. Ed.* 57 (2018) 6791–6795.
- [58] J. Ashok, M.L. Ang, S. Kawi, *Catal. Today* 281 (2017) 304–311.
- [59] M.A.A. Aziz, A.A. Jalil, S. Triwahyono, A. Ahmad, *Green Chem.* 17 (2015) 2647–2663.
- [60] J.I. Di Cosimo, V.K. Díez, M. Xu, E. Iglesia, C.R. Apesteguía, *J. Catal.* 178 (1998) 499–510.
- [61] S.E. Collins, M.A. Baltanás, A.L. Bonivardi, *J. Phys. Chem. B* 110 (2006) 5498–5507.
- [62] J. Szanyi, J.H. Kwak, *Phys. Chem. Chem. Phys.* 16 (2014) 15117–15125.
- [63] K. Coenen, F. Gallucci, B. Mezari, E. Hensen, M. van Sint Annaland, *J. CO2 Util.* 24 (2018) 228–239.
- [64] S. Eckle, H.-G. Anfang, R.J. Behm, *J. Phys. Chem. C* 115 (2011) 1361–1367.
- [65] A. Solis-Garcia, J.F. Louvier-Hernandez, A. Almendarez-Camarillo, J.C. Fierro-Gonzalez, *Appl. Catal. B-Environ.* 218 (2017) 611–620.
- [66] X. Wang, H. Shi, J.H. Kwak, J. Szanyi, *ACS Catal.* 5 (2015) 6337–6349.
- [67] B. Miao, S.S.K. Ma, X. Wang, H. Su, S.H. Chan, *Catal. Sci. Technol.* 6 (2016) 4048–4058.